scientific reports

Check for updates

OPEN

Exosomal novel-miRNA-126 mediates vascular endothelial dysfunction by targeting AhR-NLRP3 pathway in nonalcoholic steatohepatitis

Qiuhe Chen[1,5], Lifeng Ye[1,5], Liting Huang[1], Hongjing You[1], Xiaoying Yu[1], Ke Wang[1], Shengtao Xiong[4], Weiyan Liao[4], Xiao Wang[4], Haiyan Li[1] & Yang Chen[2,3]✉

Nonalcoholic steatohepatitis (NASH) is an increasingly prevalent liver disease associated with obesity and its complications. Recent studies have underscored a significant correlation between NASH and an elevated risk of cardiovascular diseases. However, the precise mechanisms of inter-organ communication between the liver and vascular endothelium are not fully understood. In this study, we established a NASH mouse model using a methionine-choline-deficient diet to investigate the role of liver-derived exosomes in modulating vascular endothelial dysfunction during NASH progression. Utilizing both in vivo and in vitro experimental approaches, we observed vascular dysfunction and activation of the NLRP3 inflammasome in NASH mice. Further analyses identified exosomal novel-miRNA-126 as a critical mediator influencing vascular endothelial dysfunction. This miRNA augments NLRP3 transcription and accelerates NLRP3 inflammasome activation by targeting the aryl hydrocarbon receptor (AhR). These findings offer novel insights into the mechanisms of liver-to-vascular communication and suggest new avenues for the prevention and therapeutic intervention of cardiovascular complications in NASH patients.

Keywords Non-alcoholic steatohepatitis (NASH), Exosome, NLRP3, Endothelial dysfunction

Nonalcoholic steatohepatitis (NASH) is characterized by hepatic steatosis accompanied by lobular inflammation and hepatocyte injury, with or without fibrosis. It represents a critical phase in the clinical continuum of nonalcoholic fatty liver disease (NAFLD), a disorder increasingly associated with obesity and its related complications[1,2]. Extensive clinical evidence indicates that patients with NASH are at a heightened risk for cardiovascular diseases (CVDs), such as heart disease and stroke. This susceptibility substantially contributes to elevated morbidity and mortality rates from cardiovascular complications[3,4].

Vascular endothelial dysfunction is the starting point and a key factor in the development and progression of many cardiovascular diseases. While evidence supports a pathological connection between vascular endothelial dysfunction and NASH, the specific mechanisms behind this link are not yet fully understood. Exosomes, small extracellular vesicles ranging from 50 to 200 nanometers in diameter, have emerged as critical players in intercellular communication, influencing both physiological and pathological states[5,6]. These vesicles, secreted by a diverse array of cell types, contain bioactive molecules including proteins, lipids, RNAs, microRNAs (miRNAs), DNAs, and other cellular components, which vary in their roles across different conditions[7,8]. Among these, exosomal miRNAs are particularly notable for their abundance and functional significance. Upon uptake by adjacent or remote cells, exosomal miRNAs can bind to the mRNA of target genes through partial sequence complementarity, significantly altering post-transcriptional gene expression[9].

[1]State Key Laboratory of Traditional Chinese Medicine Syndrome, School of Pharmaceutical Sciences, Guangzhou University of Chinese Medicine, Guangzhou 510006, Guangdong, China. [2]Chinese Medicine Guangdong Laboratory, Zhuhai 519031, Guangdong, China. [3]State Key Laboratory of Traditional Chinese Medicine Syndrome, Science and Technology Innovation Center, Guangzhou University of Chinese Medicine, Guangzhou, China. [4]School of Basic Medical Sciences, Guangzhou University of Chinese Medicine, Guangzhou 510006, Guangdong, China. [5]Qiuhe Chen and Lifeng Ye contributed equally. ✉email: ychen8@gzucm.edu.cn

While substantial evidence highlights a pathological connection between vascular endothelial dysfunction and nonalcoholic steatohepatitis (NASH), the precise mechanisms underlying this association remain elusive. Some of research have been shown that exosomal miRNAs have attracted considerable research attention due to their role in the initiation and progression of CVDs[10–12]. They serve as pivotal messengers among endothelial cells and other cell types, contributing to the pathophysiology of various diseases, including CVDs[13–16]. Previous studies have demonstrated that the activation of the NOD-like receptor family, pyrin domain containing 3 (NLRP3) inflammasome, plays a role in vascular endothelial dysfunction in CVDs[17]. The NLRP3 inflammasome, a well-characterized multiprotein complex, consists of the cytoplasmic sensor molecule NLRP3, an adaptor protein apoptosis-associated speck-like protein containing a CARD (ASC), and the effector pro-caspase-1. This complex is crucial in inflammatory responses, regulating the maturation of proinflammatory cytokines IL-1β and IL-18[15]. Given the association of exosomal miRNAs with the formation and activation of the NLRP3 inflammasome[18], our study hypothesizes that NASH liver-derived exosomal miRNAs could induce endothelial dysfunction by modulating the activation of the NLRP3 inflammasome, and aims to explore the effects and underlying mechanisms of these exosomal miRNAs on endothelial dysfunction and NLRP3 inflammasome activation.

In this study, we provide robust evidence supporting the presence of vascular endothelial dysfunction in NASH and elucidate the pivotal role of liver-derived exosomes in facilitating inter-organ communication between the liver and vascular endothelium. Our findings demonstrate that NASH liver-derived exosomes can be internalized by endothelial cells, thereby exacerbating vascular endothelial dysfunction mediated by NLRP3 inflammasome. Through in-depth research, we have identified a novel miRNA, novel-miR-126, which promotes the transcription of the NLRP3 gene and activates the NLRP3 inflammasome by specifically targeting the AhR, thus playing a significant role in NASH-associated vascular endothelial dysfunction.

Materials and methods

Animal experiments

All the procedures of the study were followed by the ARRIVE guidelines and approved by the Ethics Committee of the School of Pharmaceutical Sciences of Guangzhou University of Chinese Medicine (permit number: ZYD-2019-081). We confirmed that all experiments in this study were performed in accordance with the relevant guidelines and regulations. Male 8-week C57BL/6J mice were purchased from Nanjing Biomedical Research Institute of Nanjing University (Nanjing, China) and housed on 12/12 light-dark cycle, in a temperature-controlled room (21–25 °C) and food and water were made ad libitum. The methionine-choline-supplemented (MCS) diet and methionine-choline-deficient (MCD) diet were purchased from Trophic Animal Feed High-tech Co., Ltd., China (TP3005G, TP3005GS). Mice were randomly divided into MCS group and MCD group, which were fed MCS or MCD diet for 2–6 weeks. Then the mice were anesthetized with pentobarbital sodium solution and sacrificed. The serums were collected for AST and ALT determination. The livers were fixed with 4% paraformaldehyde (Biosharp, #BL539A) for HE staining and oil red O staining and the hearts were stored at − 80 °C for further study.

Determination of AST and ALT activities

The concentrations of AST and ALT in serum were detected by the use of commercial kits according to the manufacturer's protocols (Nanjing Jiancheng Biology, Nanjing, China; AST, #C010-2-1; ALT, #C009-2-1).

HE staining

Liver paraffin sections (4 μm) were dewaxed and stained with hematoxylin and eosin according to the manufacture's protocol (Beyotime Biotechnology, Shanghai, China, #C0105S). After staining, the sections were dehydrated with ethanol, cleared in xylene and cover-slipped with neutral balsam. The morphological changes of the liver were observed and photographed under a microscope (Olympus, Tokyo, Japan).

Oil red O staining

The frozen Sect. (4 μm) were fixed with 4% paraformaldehyde and stained with oil red O (Biotopped, Beijing, China, #Top0506) according to the manufacture's protocol. The sections were observed and photographed by the use of a microscope (Olympus, Tokyo, Japan).

Analysis of endothelial relaxation function

The analysis of endothelial relaxation function was performed as described previously[19]. The isolated thoracic aortas of 4-week MCS and MCD mice were placed in cold and oxygenated physiological saline solution (PSS). A piece of vessel with the length about 2 mm was cut and fixed to an isolated microvascular tension measurement system (DMT620M, Danish Myo Technology). PSS was continuously bubbled with a gas mixture of 95% O_2 and 5% CO_2 throughout the experiment in the bath. An optimal preload tension of 5 mN was applied to the vessel rings. After equilibrating for 1 h, the vessel rings were treated with a high-K^+ (60 mmol/L) solution to reactivation. Next, the vessel rings were contracted by phenylephrine (10^{-3} mol/L) (Sigma, #P1240000) for 5 min, and acetylcholine (ACh, 10^{-2} mol/L) (Sigma, #A6625) was subsequently used to relax the rings. After being washed, vessel relaxations in response to ACh (10^{-9}–10^{-5} mol/L) and nitroprusside (SNP, 10^{-9}–10^{-5} mol/L) (MACKLIN, #S992851) were assessed.

Immunofluorescence staining

For tissue or cell immunofluorescence staining, cardiac frozen sections (8 μm) or cell chambers were fixed in cold acetone or 4% paraformaldehyde for 15 min, rinsed with 0.05% PBST (0.05% Tween 20) (PBS: Boster Biological Technology, #AR0030; Tween 20: GBCBIO Technologies, #0777) and blocked with donkey serum

(Jackson, #017-000-121) for 1 h at room temperature. The samples were incubated overnight at 4 °C with the primary antibodies targeting eNOS (CST, #32027), ZO-1 (Invitrogen, #40-2200), ZO-2 (Invitrogen, #71-1400), VE cadherin (Abcam, #Ab33168), NLRP3 (Abcam, #Ab4207), Caspase-1 (Santa, #SC-56036), vWF (Abcam, #Ab11713) or CD31 (Santa, #SC-376764). After being washed with 0.05% PBST for three times, the slides were incubated with corresponding Alexa Fluor 488 or Alexa Fluor 555-labeled secondary antibodies for 1 h at room temperature. The sections and cells were visualized by a laser confocal microscope (LSM 800, ZEISS). Image analysis was performed by the image Pro-Plus software.

Purification and characterization of exosomes

Liver tissues of mice in MCS and MCD groups (6-week) were rinsed, cut into small pieces and homogenized at 60 HZ for 60 s (twice). The homogenates were transferred to new EP tubes and centrifuged at 2000×g for 30 min at 4 °C. The supernatant was collected and centrifuged at 10,000×g for 30 min at 4 °C (repeat this step). The supernatant was filtered with 0.22 μm microporous membranes and centrifuged at 110,000×g for 70 min at 4 °C. Then the supernatant was removed and the exosome sediment was resuspended in PBS and filtered with 0.22 μm microporous membranes again. The concentration of exosome was quantified with BCA assay (Beyotime Biotechnology, #P0012). The particle size of exosome was determined by nanoparticle tracking analysis with a Nanosight NS 300 (Malvern, Malvern, UK), and the morphology of exosome was identified with transmission electronic microscope (JEOL, Tokyo, Japan).

Western blotting assay

The Western blotting assay was performed as previously described[20]. Cells were lysed on ice and the lysates were collected and centrifuged at 12,000 rpm for 15 min at 4 °C. The concentrations of protein were quantified with BCA assay. Protein samples were separated by using 8–15% SDS-PAGE and then transferred to a PVDF membrane (Millipore, #IPFL00010). Membranes were incubated with 5% non-fat milk at room temperature for 1 h and incubated with the primary antibodies (ZO-1, Invitrogen, 40-2200; ZO-2, Invitrogen, 71-1400; NLRP3, Abcam, ab91413; Caspase-1, Santa, sc-398715; IL-1β, Abcam, ab9722; AhR, Santa, sc-133088; β-actin, Bioss, bs-0061R) overnight at 4 °C. Then the membranes were washed with TBST for 15 min and incubated with secondary antibodies at room temperature for 1.5 h. The protein bands were visualized by using an ECL Prime kit (Tanon, Shanghai, China) and analyzed with Image J software.

Cell culture and treatments

The mouse vascular endothelial cell (MVEC) EOMA cell line was obtained from ATCC. The MVECs were cultured in Dulbecco's modified eagle medium (DMEM) (Gibco, Carlsbad, CA) with 10% (v/v) fetal bovine serum (FBS) and 1% (v/v) penicillin-streptomycin and incubated at 37 °C under 5% CO_2. MVECs were pretreated with or without 10 nM MCC950 for 30 min or 80 μM dynasore for 1 h, followed by 120 μg/mL liver-derived exosomes treatment.

Transendothelial electrical resistance (TEER) measurement

TEER measurement was performed as previously described[21]. MVECs were seeded on top of trans-well chambers (LABSELECT, #14312). TEER value was measured by Millicell ERS-2 epithelial volt-ohmmeter (Millipore, USA) after exosomes treatment for 24 h. TEER reading was recorded immediately. TEER values are calculated as: TEER = resistance × filter area ($\Omega \cdot cm^2$).

Measurement of endothelial permeability

To evaluate the permeability of the cells, we measured the transmembrane movement of fluorescein isothiocyanate (FITC)-conjugated dextran (Sigma, #46945) across monolayers of MVECs as previously described[21]. Initially, MVECs were cultivated on transwell inserts within 24-well plates. After treated with exosomes for 24 h at 37 °C, MVECs monolayer permeability was measured by adding 100 μL of FITC-dextran 40 kDa (1 mg/mL) to the upper chamber. Samples from the upper and lower compartments were measured by fluorescent plate reader using excitation and emission wavelengths of 485 and 535 nm, respectively.

MiRNA deep-sequencing

Live exosomal miRNAs were profiled by the small RNA sequencing analysis (Illumina Inc., San Diego, CA, USA) and the difference analysis between CL^{Exo} (liver exosomal miRNA of mice in MCS group) and ML^{Exo} (liver exosomal miRNA of mice in MCD group) groups was performed by the use of DESeq R package. Prediction of miRNA targets and identification of miRNA binding sites were performed using Randfold tools.

Real-time quantitative PCR

To detect the level of novel-miR-1268, novel-miR-126, novel-miR-499, novel-miR-1698 and U6 in liver exosomes and the mRNA level of NLRP3 and β-actin in MVECs, the total RNAs in liver exosomes or MVECs were isolated using TRIzol reagent and reverse transcribed using a miRNA first-strand cDNA synthesis kit (Sangon, Shanghai, China) according to the manufacturer's protocols. RT-qPCR was performed using a TB Green™ Premix Ex Taq™ (Takara, Kyoto, Japan) according to the manufacturer's protocols. Relative miRNA expression levels were calculated using the comparative threshold (CT) method. Results of miRNA were normalized to U6 in liver exosomes or MVECs and the result of NLRP3 were normalized to β-actin in MVECs. The primers were purchased from Sangon Bio-tech, and the sequences are listed in Table 1.

	Forward	Reverse
NLRP3	AGGAGAATGGACCTGCAAGC	TCTACCATCATCCAGCCTTGG
β-actin	CCCATCTATGAGGGTTACGC	TTTAATGTCACGCACGATTTC
Novel-miR-1268	TAGGGCTGGAGAGATGGCTCA	–
Novel-miR-126	AGGGCTGGAGAGATGGCTC	–
Novel-miR-499	AAGGGCTGGAGAGATGGCTC	–
Novel-miR-1698	GGGGCTGGAGAGATGGCT	–
U6	CTCGCTTCGGCAGCACA	–

Table 1. Primer sequences.

Transfection of novel-miR-126 mimic

For the functional analysis of novel-miR-126, MVECs were transfected with either a 5-FAM-labelled novel-miR-126 mimic or a negative control mimic. The sequences for the novel-miR-126 mimic were as follows: sense 5′-AGGGCUGGAGAGAUGGCUCAGUGC-3′, antisense 5′-ACUGAGCCAUCUCUCCAGCCCUUU-3′. The negative control mimic sequence was: sense 5′-UUCUCCGAACGUGUCACGUTT-3′, antisense 5′-ACGUGA CACGUUCGGAGAATT-3′, both provided by GenePharma, Shanghai, China. The transfection was performed at a final concentration of 50 nM using Lipofectamine 3000 (Invitrogen, L3000015), following the manufacturer's protocol. Transfection efficiency was assessed using confocal microscopy. After a 48 h incubation period, the cells were collected for subsequent RT-PCR or western blot analysis.

Statistical analysis

All data are presented as the mean ± SEM. All statistical analyses were performed using GraphPad Prism 8. Two independent sample *t*-test was used to compare the measurement data of the two groups and one-way ANOVA followed by Tukey's multiple comparisons test when more than two groups were present. $P < 0.05$ was considered statistically significant.

Results

Vasodilation dysfunction was observed in NASH mice

8-week male C57BL/6 N mice were fed with MCS or MCD diet for 2 to 6 weeks to establish NASH mouse model. The results of HE and oil red O staining of liver showed that MCD diet administration induced severe fat vacuoles and lipid accumulation (Fig. 1A), and 6-week mice exhibited more severe hepatic steatosis and inflammatory infiltration when compared with 2-week mice. Besides, the concentrations of serum ALT and AST in mice of MCD group were substantially increased when compared with MCS group (Fig. 1B). However, there was no significant difference between the 2 week group and 6 week group. These results suggested that NASH mouse model was successfully established. Concurrently, aortic tension assessments revealed the presence of vasodilation dysfunction in NASH mice (MCD diet for 4 weeks), with endothelium-dependent relaxation in response to acetylcholine (ACh) being notably compromised in the MCD group, whereas relaxation mediated by smooth muscle in response to sodium nitroprusside (SNP) exhibited no significant difference among the groups (Fig. 1C).

Disruption of inter-endothelial junction occurred in the coronary arteries of NASH mice

Endothelial cell-to-cell junctions are pivotal in maintaining vascular homeostasis. Serving as critical endothelial barrier structures, the interendothelial junctions, including tight junction (TJ) proteins like zonula occludens-1/2 (ZO-1/2) and adherens junction (AJ) proteins like vascular endothelial-cadherin (VE-Cadherin), are essential for regulating paracellular permeability. Besides, endothelial nitric oxide synthase (eNOS) is critical in the regulation of vascular function, and can generate both nitric oxide (NO) and superoxide ($O_2^{\cdot-}$), which are key mediators of cellular signalling[22]. Consequently, the downregulation of ZO-1/2, VE-Cadherin as well as eNOS is considered as marker events of vascular dysfunction. We have observed and proved the vasodilation dysfunction in NASH mice. However, it remains to be elucidated whether microvascular alterations occur in NASH mice. To determine if the vascular interendothelial junctions are compromised in NASH mice, the immunofluorescence co-localization of ZO-1/2, VE-Cadherin (green), eNOS and endothelial specific marker vWF (red) respectively in the coronary arteries were detected, and found that the expressions of ZO-1/2 (Fig. 2A, B), eNOS and VE-Cadherin (Fig. 2C, D) were decreased in mice of MCD group in contrast to contemporaneous mice in MCS group. Further analysis of the data from the 2-week and 6-week groups revealed significant differences in the levels of ZO-1 and eNOS, while no significant statistical differences were observed in the levels of ZO-2 and VE-Cadherin.

NLRP3 inflammasome activation occurred in the coronary arteries of NASH mice

The role of NLRP3 inflammasome in regulating the paracellular permeability of vascular endothelium has been previously reported[23]. Pearson correlation analysis was conducted to examine the relationships between NLRP3 and TPJ1, TPJ2, NOS3, and CDH5 genes, indicating significant correlations, particularly between NLRP3, TPJ1, TPJ2, and CDH5 (Fig. 3A). Subsequently, immunofluorescence co-localization was performed to determine whether activation of the NLRP3 inflammasome contributed to endothelial dysfunction and vascular injury within the coronary arteries during the progression of NASH. The results demonstrated that the co-localization

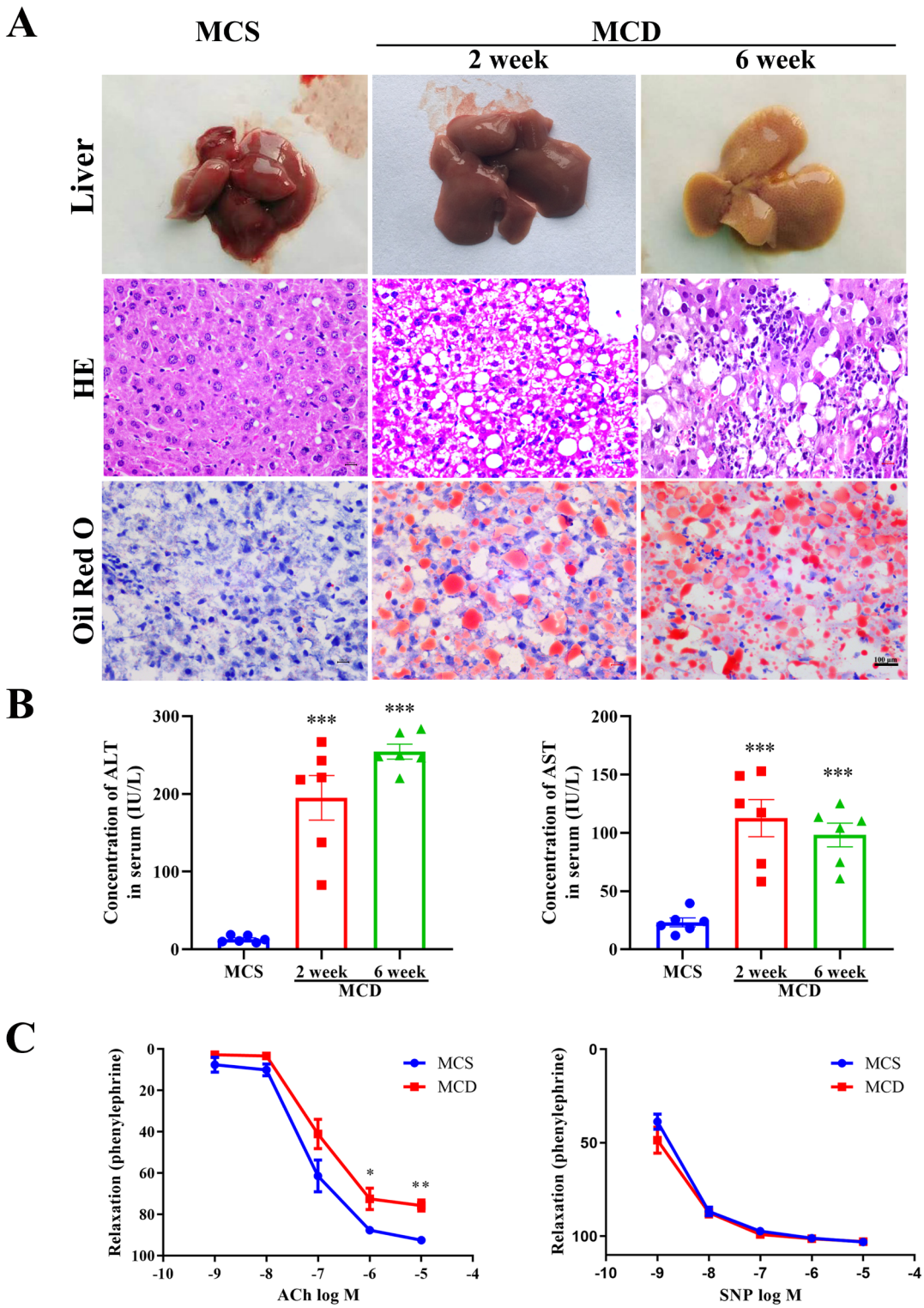

Fig. 1. NASH is associated with vascular endothelial dysfunction in mice fed with MCD diet. (**A**) Representative pictures of liver, HE staining and oil red O staining. (**B**) Serum level of ALT and AST. (**C**) Response curve to ACh and SNP in thoracic aortic rings from MCS diet and MCD diet fed mice (4 week). Data are expressed as mean ± SEM, $n = 6$ per group. $^{*}P < 0.05$, $^{**}P < 0.01$, $^{***}P < 0.001$ versus MCS group. Scale bar = 100 μm.

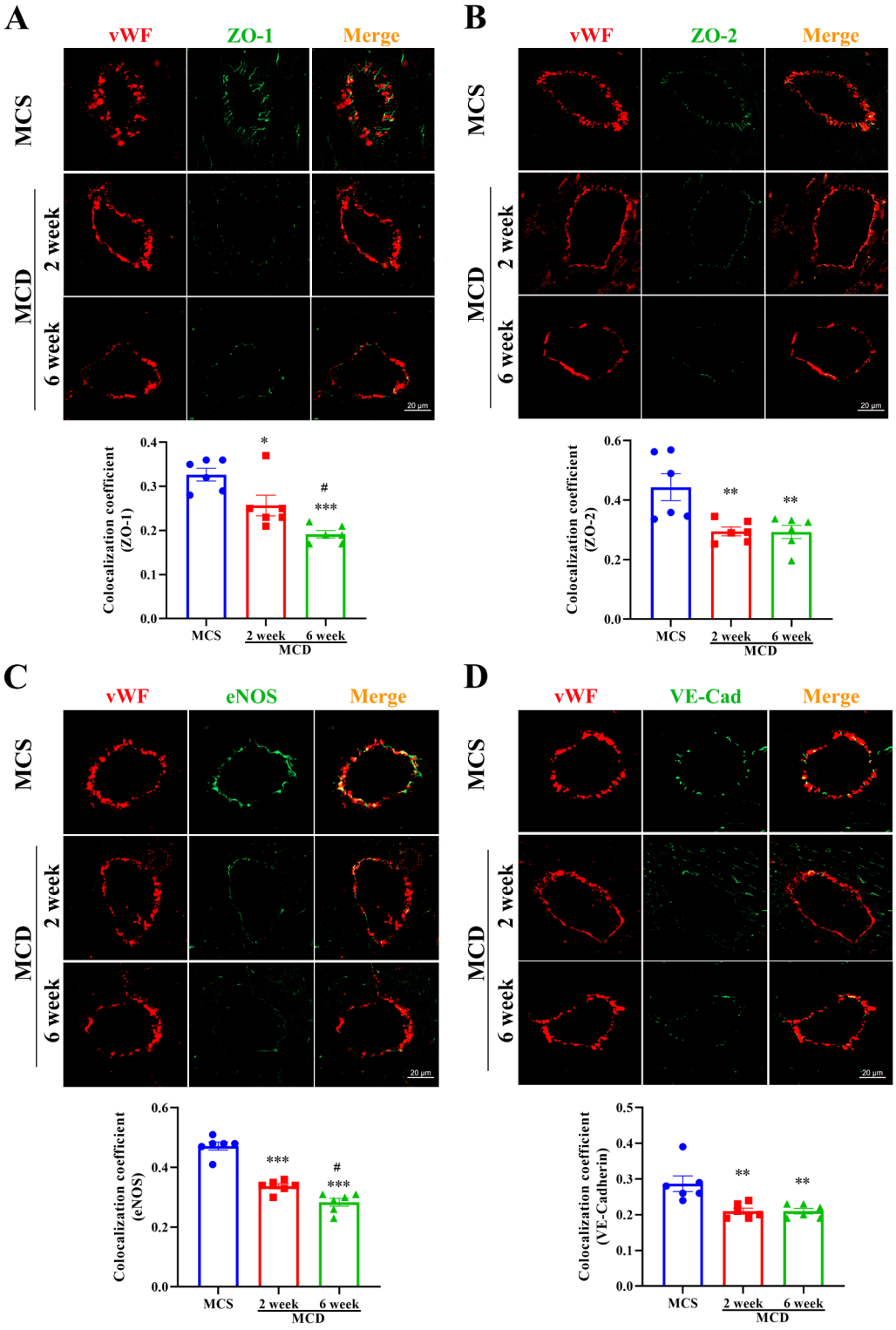

Fig. 2. Disruption of inter-endothelial junction of coronary arteries in NASH mice. (**A**) Representative fluorescent confocal images of ZO-1 (green) and vWF (red) and the summarized data of the colocalization coefficient. (**B**) Representative fluorescent confocal images of ZO-2 (green) and vWF (red) and the summarized data of the colocalization coefficient. (**C**) Representative fluorescent confocal images of eNOS (green) and vWF (red) and the summarized data of the colocalization coefficient. (**D**) Representative fluorescent confocal images of VE-Cadherin (green) and vWF (red) and the summarized data of the colocalization coefficient. Data are expressed as mean ± SEM, $n = 6$ per group. $^{*}P < 0.05$, $^{**}P < 0.01$, $^{***}P < 0.001$ versus MCS group. $^{\#}P < 0.05$ versus 2-week MCD group. Scale bar = 20 μm.

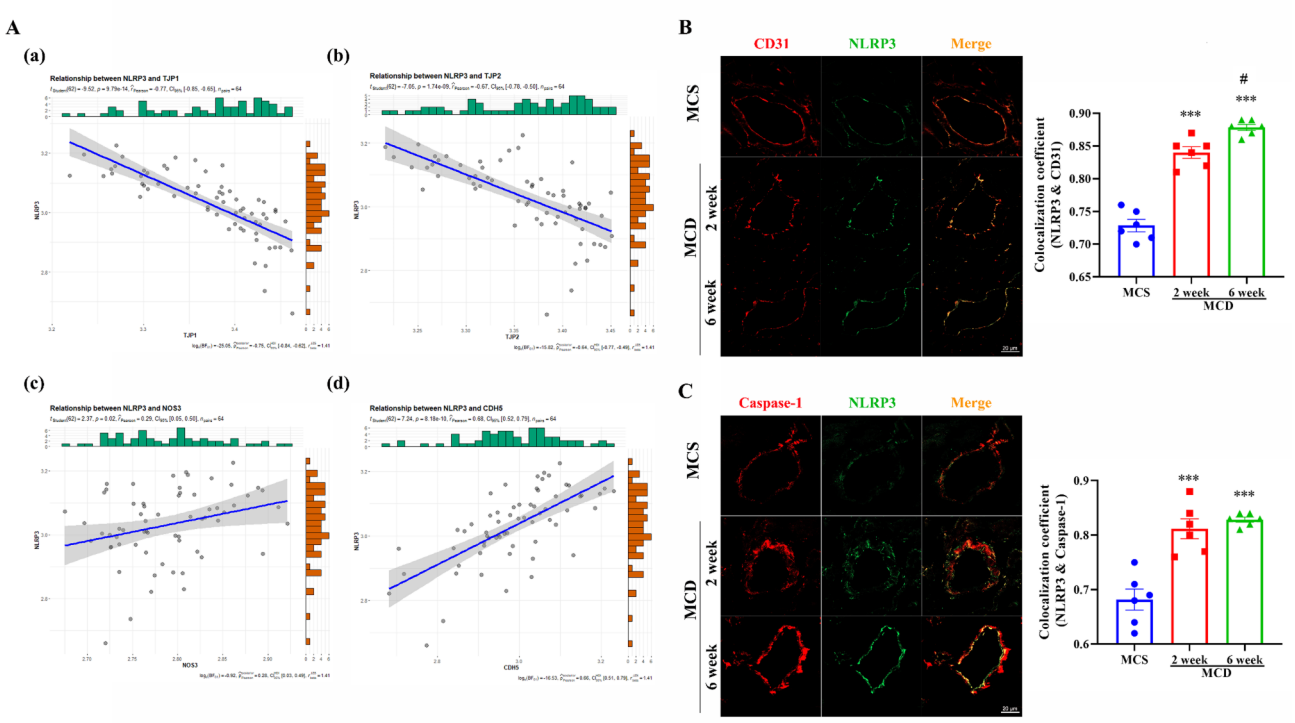

Fig. 3. Activation of NLRP3 inflammasome occurred in coronary arteries in NASH mice. (**A**) Pearson's correlations were used for statistical comparisons. (**B**) Representative fluorescent confocal images of NLRP3 (green) and CD31 and the summarized data of the colocalization coefficient. Scale bar = 20 μm. (**C**) Representative fluorescent confocal images of NLRP3 (green) and caspase-1 (red) and the summarized data of the colocalization coefficient. Scale bar = 20 μm. Data are expressed as mean ± SEM, $n = 6$ per group. $^{**}P < 0.01$ versus MCS group. $^{\#}P < 0.05$ versus 2-week MCD group.

coefficient between NLRP3 (green) with CD31 (red), a surface marker of endothelial cells, as well as NLRP3 (green) and caspase-1 (red), were markedly elevated in NASH mice (Fig. 3B, C). Additionally, a significant difference in the expression levels of NLRP3 was observed between the 2-week group and the 6-week group.

NASH liver-derived exosomes induced vascular endothelial dysfunction and NLRP3 inflammasome activation in Naive mice

As the well-known mediators of intercellular communication, exosomes have been reported that participate in regulating vascular permeability by targeting junction proteins[24]. To elucidate the potential association between vascular endothelial dysfunction and exosomes in NASH mice, the exosomes derived from the liver homogenate of mice in MCS or MCD group were therefore isolated using ultracentrifugation and subsequently administered into naive mice via caudal vein for 48 h (Fig. 4A). The presence of saucer-shaped vesicles in liver-derived exosome preparation were observed by transmission electron microscopy (TEM) and a diameter distribution profile ranging from 50 nm to 200 nm was measured (Fig. 4B). The vasodilation levels in response to ACh and SNP of thoracic aortic rings gained from mice in CL^{Exo} or ML^{Exo} group showed that endothelial-dependent vasodilation in response to ACh was impaired in ML^{Exo} treated mice, while there was no significant difference in endothelial-independent vasodilation in response to SNP (Fig. 4C). Furthermore, in comparison to the vehicle and CL^{Exo} group, the co-localization coefficients of NLRP3 (green) with CD31 (red) and with caspase-1 (red) were markedly increased in ML^{Exo} group (Fig. 4D, E).

NASH liver-derived exosomes induce endothelial barrier dysfunction via NLRP3 inflammasome activation in vitro

In vitro experiments on MVECs were conducted to further investigate the role of NASH liver-derived exosomes in NLRP3 inflammasome activation and endothelial dysfunction. MVECs were treated with PBS, CL^{Exo} or ML^{Exo} for 24 h respectively. As shown in Fig. 5A, the mRNA expression of NLRP3 in ML^{Exo} group was significantly increased when compared with control and CL^{Exo} group, suggesting that exosomes derived from NASH mice would up-regulate the NLRP3 gene transcription of MVECs. Further immunofluorescence co-localization analysis of caspase-1 (red) and NLRP3 (green) in MVECs was performed, revealing that ML^{Exo} could remarkedly promote the formation of NLRP3 inflammasome (Fig. 5B). In addition, ML^{Exo} increased the maturation of proinflammatory cytokine IL-1β, contrasting with the control and CL^{Exo} groups (Fig. 5C), and suggested that ML^{Exo} could induce the activation of NLRP3 inflammasome. We also detected the TEER values,

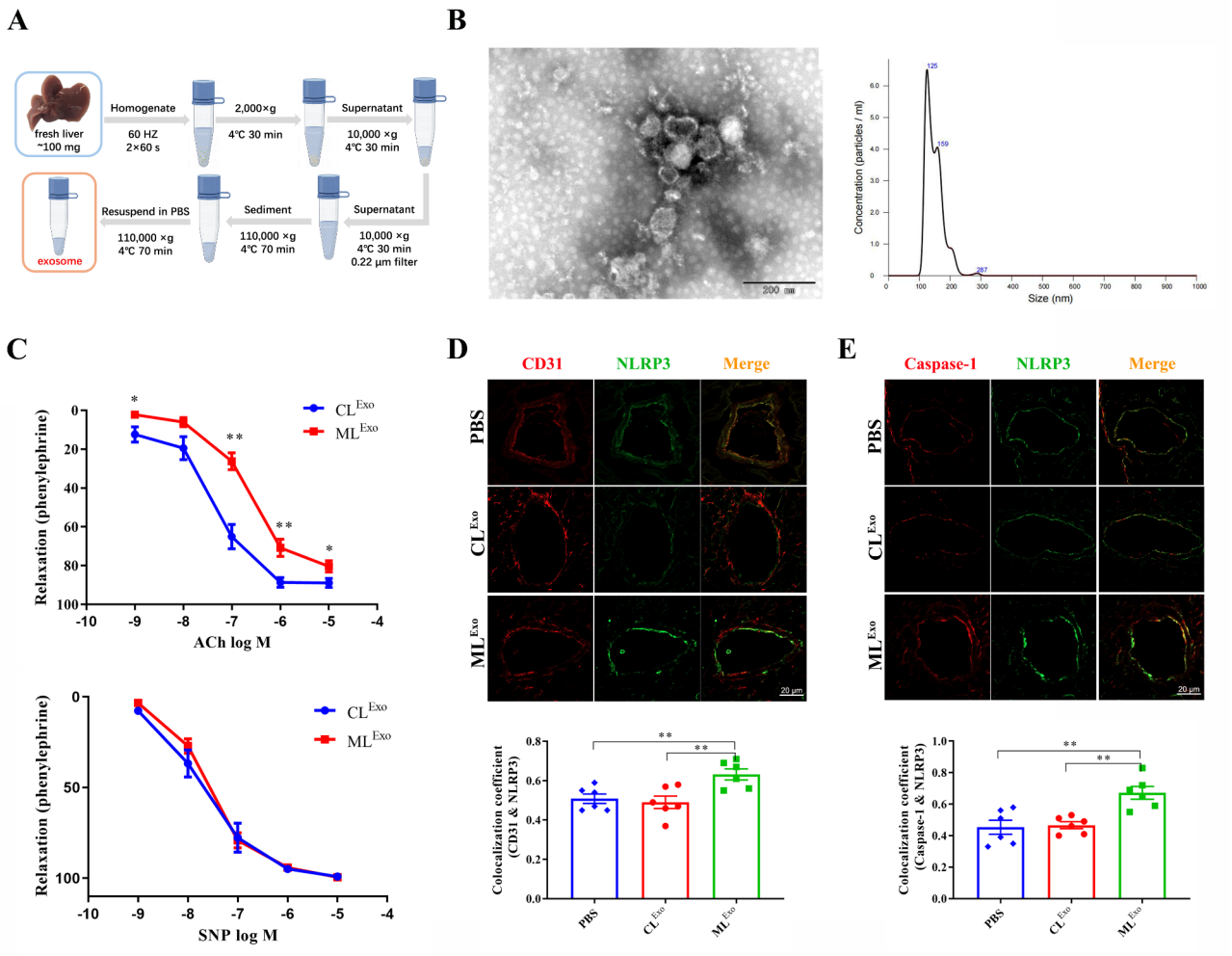

Fig. 4. NASH liver-derived exosomes induce vascular endothelial dysfunction and NLRP3 inflammasome activation in naive mice. (**A**) The isolation method of liver exosomes. (**B**) Representative electron microscopic image of exosomes and size distribution analysis of exosomes. Scale bar = 200 nm. (**C**) Response curve to ACh and SNP in thoracic aortic rings from mice treated with CL^{Exo} or ML^{Exo}. (**D**) Representative fluorescent confocal images of NLRP3 (green) and CD31 (red) and the summarized data of the colocalization coefficient. Scale bar = 10 μm. (**E**) Representative fluorescent confocal images of NLRP3 (green) and caspase-1 (red) and the summarized data of the colocalization coefficient. Scale bar = 10 μm. Data are expressed as mean ± SEM, $n = 6$ per group. $^{*}P < 0.05$, $^{**}P < 0.01$, versus CL^{Exo} group. Note: CL^{Exo} (liver exosomal miRNA of mice in MCS group) and ML^{Exo} (liver exosomal miRNA of mice in MCD group).

a parameter that remains elevated under conditions of endothelial monolayer integrity and correlates with the expression levels of proteins at inter-endothelial junctions. As shown in Fig. 5D, compared to control and CL^{Exo} group, ML^{Exo} treatment resulted in a significant decline in TEER values. Notably, this decline was substantially reversed by pretreatment with MCC950, a specific inhibitor of the NLRP3 inflammasome. Consistent with these findings, a permeability assay using 40-kDa dextran-FITC revealed that MVECs exposed to ML^{Exo} displayed increased permeability, a phenotype that was mitigated by MCC950 treatment (Fig. 5E). Moreover, immunofluorescence staining demonstrated that ML^{Exo} reduced the expression of ZO-1 in MVECs, while this effect could be abolished by MCC950 (Fig. 5F).

Exosomal novel-miR-126 mediating NLRP3 inflammasome activation and endothelial barrier dysfunction in vitro

To further determine the exosomal components responsible for vascular endothelial barrier dysfunction, miRNA deep-sequencing between CL^{Exo} and ML^{Exo} and the expression profiles of miRNA were conducted. As shown in Fig. 6A, a comparative analysis revealed 412 down-regulated and 416 up-regulated miRNAs, indicating significant differences in expression. Studies have shown that AhR plays a key role in regulating NLRP3 transcription by binding directly to its promoter region[25]. We utilized Pearson correlation analysis to assess the relationship between NLRP3 and the AhR gene, discovering a strong negative correlation between their expression levels (Fig. 6B). Subsequently, we further investigated whether endothelial barrier dysfunction

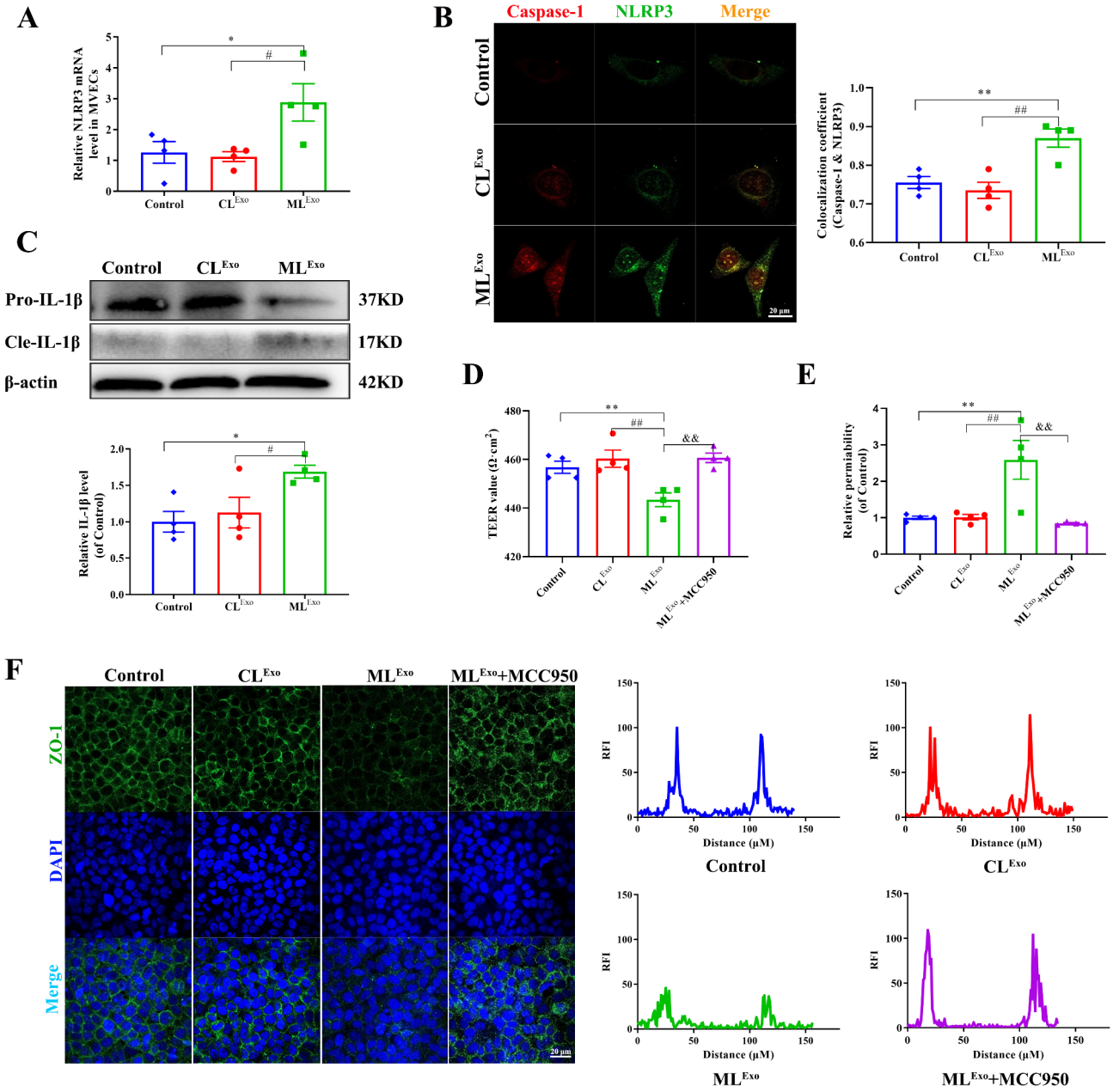

Fig. 5. NASH liver-derived exosomes induce endothelial barrier dysfunction via activating NLRP3 inflammasome in vitro. (**A**) The mRNA level of NLRP3 was analyzed by qPCR. (**B**) Representative fluorescent confocal images of NLRP3 (green) and caspase-1 (red) in MVECs and the summarized data of the colocalization coefficient. Scale bar = 20 μm. (**C**) Pro-IL-1β and cleaved IL-1β expression levels were analyzed by Western blotting and the relative protein expression levels were determined by densitometric analysis. (**D**) TEER value was measured. (**E**) The permeability of endothelial cell to 40-kDa dextran-FITC for 1 h was measured. (**F**) Representative fluorescent images of ZO-1 (green). Scale bar = 20 μm. Data are expressed as mean ± SEM, $n = 4$ per group. $^{*}P < 0.05$, $^{**}P < 0.01$ versus Control group; $^{\#}P < 0.05$, $^{\#\#}P < 0.01$ versus CL^{Exo} group; $^{\&\&}P < 0.01$ versus ML^{Exo} group. Note: CL^{Exo} (liver exosomal miRNA of mice in MCS group) and ML^{Exo} (liver exosomal miRNA of mice in MCD group).

induced by ML^{Exo} was regulated by AhR-NLRP3 axis by miRNAs. The miRNA target prediction was performed and a number of putative target miRNAs were shown in the miRNAs-gene-heatmap (Fig. 6C). Among them, novel-miR-1268, novel-miR-126, novel-miR-499 and novel-miR-1698 were selected for further validation via miScript PCR System due to their high log2FC value (Fig. 6D). The results showed that all of these miRNAs were expressed at significantly higher levels in ML^{Exo} group compared to the CL^{Exo} group, which had a high concordance with the results of miRNA-seguencing. In addition, the expression level of novel-miR-126 in MVECs exposed to ML^{Exo} was much higher than that in the control and CL^{Exo} groups, while pre-treatment with 80 μM dynasore (an endocytosis inhibitor) for 1 h could significantly block this effect (Fig. 6E). Through

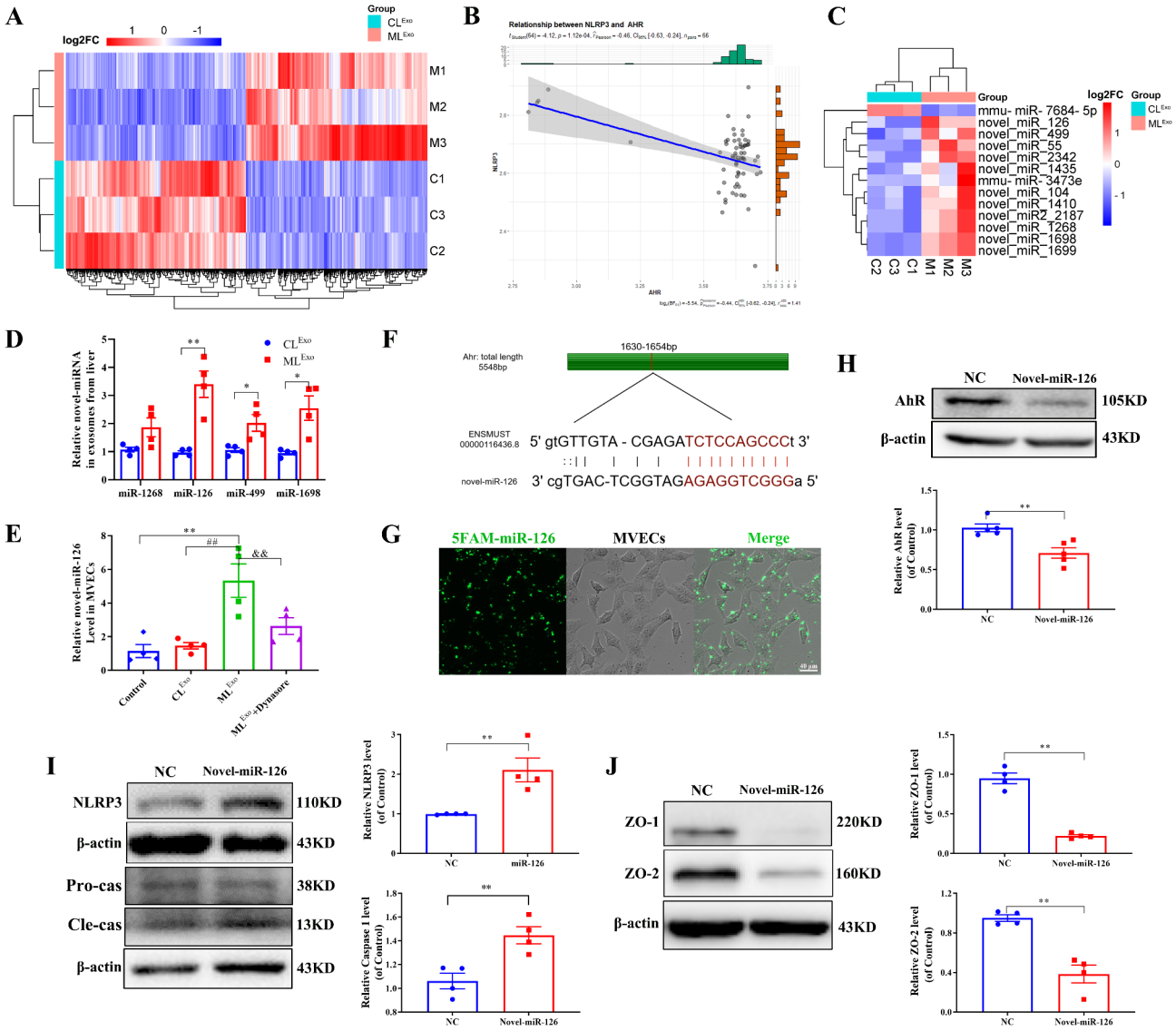

Fig. 6. Exosomal novel-miR-126 mediating NLRP3 inflammasome activation and endothelial barrier dysfunction in vitro. (**A**) The heat map of differential expressed miRNAs between CL^{Exo} and ML^{Exo}. (**B**) Pearson's correlations analysis between NLRP3 and AhR. (**C**) The miRNAs-gene-network targeting AhR. (**D**) qPCR analysis of novel-miRNAs expression levels in CL^{Exo} and ML^{Exo}. (**E**) Expression level of novel-miR-126 in MVECs. (**F**) The binding site of AhR with novel-miR-126. (**G**) The transfection efficiency of novel-miR-126 mimic. Scale bar = 40 μm. (**H**–**J**) Western blotting analysis of AhR, NLRP3, caspase-1, ZO-1 and ZO-2 expression levels and the relative protein expression levels were determined by densitometric analysis. Data are expressed as mean ± SEM, $n = 4$ per group. $^{**}P < 0.01$ versus Control group; $^{\#\#}P < 0.01$ versus CL^{Exo} group; $\&\&P < 0.01$ versus ML^{Exo} group. Note: CL^{Exo} (liver exosomal miRNA of mice in MCS group) and ML^{Exo} (liver exosomal miRNA of mice in MCD group).

bioinformatics analysis, the binding site of novel-miR-126 to the AhR gene was predicted, which further proved the regulatory effect novel-miR-126 to AhR gene (Fig. 6F). To reveal the functional effects of novel-miR-126 on MVECs, FAM-labelled novel-miR-126 mimics were transfected into MVECs (Fig. 6G), finding that the expression of AhR protein significantly decreased in MVECs overexpressing novel-miR-126 (Fig. 6H), accompanied by up-regulation of NLRP3 expression and activation of caspase-1 (Fig. 6I) as well as the down-regulation of ZO-1 and ZO-2 (Fig. 6J).

Discussion

In this study, we present compelling evidence that vascular endothelial dysfunction is a consequence of NLRP3 inflammasome activation within the vascular endothelium, induced by exosomes originating from the liver of NASH-afflicted mice. Further, through miRNA deep-sequencing techniques followed by exhaustive bioinformatics analyses, we have identified novel miR-126 as a critical exosomal bioactive molecule. This

miRNA directly binds to the aryl hydrocarbon receptor (AhR) gene, reducing its expression and subsequently stimulating the transcription of NLRP3 and the activation of the NLRP3 inflammasome, which leads to vascular endothelial dysfunction.

Clinical evidence indicates that patients with nonalcoholic steatohepatitis (NASH) are at twice the risk of developing cardiovascular diseases (CVDs), underscoring a significant correlation between NASH and vascular endothelial dysfunction[26]. In our current study, we observed notable vascular endothelial dysfunction in a NASH mouse model characterized by distinct morphological changes, hepatic fat accumulation, and elevated transaminase levels in the circulation, as depicted in Fig. 1A–C. Previous research has established an association between NASH and impaired flow-mediated dilation of the brachial artery, further affirming the presence of vascular endothelial dysfunction[27]. The endothelium, which is vital for regulating vascular tone and maintaining vascular homeostasis, typically exhibits the initial signs of dysfunction in most CVDs. Our findings demonstrate that endothelium-dependent vasodilation, in response to acetylcholine (ACh) and sodium nitroprusside (SNP), is compromised in NASH mice, a condition that occurs independently of vascular smooth muscle function. Additional analysis of the coronary artery endothelial function in NASH mice revealed significant reductions in the protein levels of ZO-1/2, endothelial nitric oxide synthase (eNOS), and vascular endothelial (VE)-cadherin, as shown in Fig. 2. These observations collectively suggest that vascular endothelial damage is a consistent feature in NASH, aligning with prior studies.

Recent years have seen significant research focused on the mechanisms responsible for the impairment of cellular junctions within endothelial lesions mediated by inflammation. Within this domain, the role of the NLRP3 inflammasome has garnered considerable interest in the scientific community. Numerous studies have identified the NLRP3 inflammasome as playing a critical role in the initial stages of vascular endothelial dysfunction linked to metabolic disorders[28,29]. Additionally, Pearson correlation analysis has revealed strong associations between NLRP3 and several key endothelial markers, including TPJ1 (ZO-1), TPJ2 (ZO-2), NOS3 (eNOS), and CDH5 (VE-cadherin). Our findings demonstrate a significant increase in NLRP3 expression and NLRP3 inflammasome formation in the coronary artery endothelium as NASH progresses, corroborating earlier studies as shown in Fig. 3B, C. These results indicate that vascular endothelial dysfunction in NASH is intricately linked with NLRP3 inflammasome activation. However, the specific pathways through which vascular endothelial dysfunction manifests in NASH remain to be fully elucidated. This suggests the existence of complex inter-organ communication mechanisms between the liver and the endothelium, which regulate NLRP3 inflammasome activation and contribute to the onset of vascular endothelial dysfunction. In addition, further analysis of the differences between the 2-week and 6-week MCD diet groups was made, revealing that compared with 2-week mice, 6-week mice exhibit more severe hepatic steatosis and inflammatory infiltration. And there are statistically significant differences in the protein level of ZO-1, eNOS and NLRP3, which indicates that as the duration of the MCD diet increases, hepatic steatosis and inflammatory infiltration become more severe, which in turn leads to a greater degree of vascular dysfunction in the mice. However, there are no significant differences in the protein level of ZO-2 and VE-cadherin, which may be related to large individual differences and a small sample size.

Recent advancements have increasingly highlighted the crucial role of exosomes as key regulators of intercellular communication in nonalcoholic steatohepatitis (NASH)[30,31]. Notably, a recent study has shown that exosomes derived from hepatocytes facilitate the M1 polarization and activation of macrophages during NASH, underscoring the significant role of liver-derived exosomes in mediating proinflammatory responses[32]. In our current research, we demonstrate that hepatocyte-derived exosomes, specifically ML^{Exo}, can induce significant vascular endothelial dysfunction by modulating the activation of the NLRP3 inflammasome. This observation supports the hypothesis that exosome-mediated material transfer is fundamental to the inter-organ communication between the liver and vascular endothelium in NASH, as illustrated in Figs. 4 and 5. Our results are consistent with recent findings that hepatocyte-derived extracellular vesicles play a contributory role in endothelial inflammation and atherogenesis[33].

Non-coding RNAs, particularly microRNAs (miRNAs), have garnered significant interest in both basic and translational biomedical research over the past few years, primarily due to their regulatory impact on gene expression and their potential as biomarkers for diseases[15,34]. Recent studies have elucidated the biological effects of hepatic exosomal miRNAs in the context of nonalcoholic steatohepatitis (NASH)[20,32]. Building on these findings, we performed deep sequencing of exosomal miRNAs derived from control liver exosomes (CL^{Exo}) and NASH liver exosomes (ML^{Exo}), with the results of differentially expressed miRNAs presented in Fig. 6A. The aryl hydrocarbon receptor (AhR), a multifunctional ligand-activated transcription factor, plays a dual role in NASH: deregulation of AhR may contribute to hepatic steatosis and inflammation, whereas AhR-targeted genes such as CD36, SOCS3, and FGF21 have been implicated in protective mechanisms against NASH[35]. Notably, AhR also acts as a significant negative regulator of NLRP3 transcription and physiologically suppresses the NLRP3 inflammasome through its interaction with the xenobiotic response element (XRE) in the NLRP3 promoter[25]. This regulatory role was substantiated by Pearson correlation analysis in our study, as shown in Fig. 6B. In this study, we identified miRNAs that significantly target AhR and compared their expression levels between the CL^{Exo} and ML^{Exo} groups, detailed in Fig. 6C, D. Notably, novel-miR-126 emerged as the most abundantly expressed miRNA in the ML^{Exo} group, thereby pinpointing it as a crucial exosomal miRNA cargo in the regulation of NLRP3 inflammasome activation. Our experimental results revealed that microvascular endothelial cells (MVECs) overexpressing novel-miR-126 displayed increased susceptibility to endothelial damage and NLRP3 inflammasome activation, mediated through the suppression of AhR, as depicted in Fig. 6H–J. Collectively, our findings demonstrate that NASH liver-derived exosomal novel-miR-126 promotes endothelial dysfunction by directly binding to AhR mRNA, thereby inducing NLRP3 transcription and activating the NLRP3 inflammasome.

In summary, our study demonstrates that exosomes are instrumental in inducing significant vascular endothelial dysfunction, an effect mediated through the upregulation of NLRP3 gene transcription and

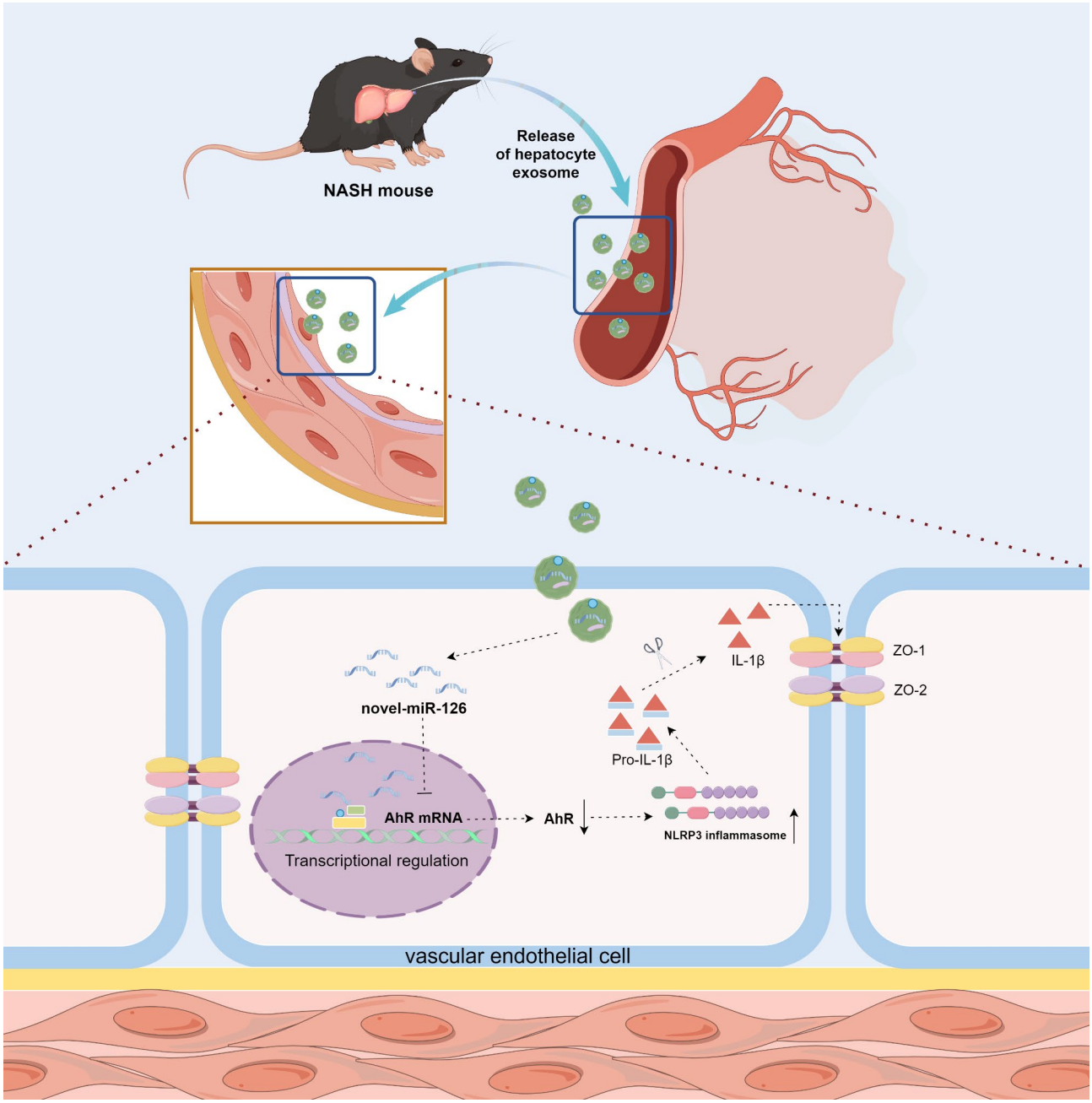

Fig. 7. The mechanisms of vascular damage in NASH mouse. In NASH mice, liver-derived exosomes are released into the systemic circulation. As one of the contents of exosomes, noval-miRNA-126 enters vascular endothelium and binds to a specific site on AhR mRNA, thereby affecting AhR protein expression. The downregulation of AhR leads to the activation of NLRP3 inflammasome, which further promotes the cleavage of Pro IL-1β into mature IL-1β. Then IL-1β further affects the tight junction proteins ZO-1/2 in vascular endothelium, leading to impaired vascular endothelial function.

the subsequent activation of the NLRP3 inflammasome in the context of NASH. In addition, our in-depth investigation has uncovered that the miRNA novel-miR-126, a pivotal exosomal component, facilitates the transcription of the NLRP3 gene and triggers the activation of the NLRP3 inflammasome by specifically targeting AhR (Fig. 7), which sheds new light on the intricate inter-organ communication mechanisms between the liver and the vascular endothelium and offers promising directions for the development of preventive and therapeutic strategies for CVDs in NASH patients. However, the the potential role of novel-miR-126 in NASH and vascular dysfunction have only been verified in vitro, and there is still a lack of in vivo functional validation at the NASH related animal model, which would help to better clarify the role of novel-miR-126 in NASH and vascular dysfunction.

Data availability

Data and analyzed results related to the MiRNA deep-sequencing can be found in the Supplementary Tables 1 and Table 2. The Pearson's correlations analysis transcriptomic datasets were retrieved from the Gene Expression Omnibus: GSE43292 (n =64), GSE151158 (n=66). Other datasets used and/or analyzed during the current study are available from the corresponding author upon reasonable request.

Received: 18 November 2024; Accepted: 18 March 2025
Published online: 25 March 2025

References

1. Bhatia, L. S., Curzen, N. P., Calder, P. C. & Byrne, C. D. Non-alcoholic fatty liver disease: A new and important cardiovascular risk factor? *Eur. Heart J.* **33**, 1190–1200 (2012).
2. Younossi, Z. M., Marchesini, G., Pinto-Cortez, H. & Petta, S. Epidemiology of nonalcoholic fatty liver disease and nonalcoholic steatohepatitis: Implications for liver transplantation. *Transplantation* **103** (2019).
3. Targher, G., Byrne, C. D., Lonardo, A., Zoppini, G. & Barbui, C. Non-alcoholic fatty liver disease and risk of incident cardiovascular disease: A meta-analysis. *J. Hepatol.* **65**, 589–600 (2016).
4. Kasper, P. et al. NAFLD and cardiovascular diseases: A clinical review. *Clin. Res. Cardiol.* **110**, 921–937 (2021).
5. Dini, L. et al. Microvesicles and exosomes in metabolic diseases and inflammation. *Cytokine Growth Factor Rev.* **51**, 27–39 (2020).
6. Cunha, Rocha, K., Ying, W. & Olefsky, J. M. Exosome-mediated impact on systemic metabolism. *Annu. Rev. Physiol.* **86**, 225–253 (2024).
7. Krylova, S. V. & Feng, D. The machinery of exosomes: Biogenesis, release, and uptake. *Int. J. Mol. Sci.* **24**, 1337 (2023).
8. Pegtel, D. M., Gould, S. J. & Exosomes *Annu. Rev. Biochem.* **88**, 487–514 (2019).
9. Zheng, D. et al. The role of exosomes and Exosomal MicroRNA in cardiovascular disease. *Front. Cell. Dev. Biol.* **8**, 616161 (2021).
10. Lawson, C., Vicencio, J. M., Yellon, D. M. & Davidson, S. M. Microvesicles and exosomes: New players in metabolic and cardiovascular disease. *J. Endocrinol.* **228**, R57–R71 (2016).
11. Zhang, H. et al. Serum exosomes mediate delivery of arginase 1 as a novel mechanism for endothelial dysfunction in diabetes. *Proc. Natl. Acad. Sci.* **115**, E6927–E6936 (2018).
12. Qiu, D. et al. Fenugreek extract improves diabetes-induced endothelial dysfunction via the arginase 1 pathway. *Food Funct.* **15**, 3446–3462 (2024).
13. Kir, D., Schnettler, E., Modi, S. & Ramakrishnan, S. Regulation of angiogenesis by microRNAs in cardiovascular diseases. *Angiogenesis* **21**, 699–710 (2018).
14. Li, J. et al. Exosomes derived from mesenchymal stem cells attenuate the progression of atherosclerosis in ApoE−/− mice via miR-let7 mediated infiltration and polarization of M2 macrophage. *Biochem. Biophys. Res. Commun.* **510**, 565–572 (2019).
15. Aghabozorgi, A. S. et al. Circulating exosomal MiRNAs in cardiovascular disease pathogenesis: New emerging hopes. *J. Cell. Physiol.* **234**, 21796–21809 (2019).
16. Li, C. et al. Roles and mechanisms of exosomal non-coding RNAs in human health and diseases. *Signal. Transduct. Target. Ther.* **6**, 383 (2021).
17. Chen, Y. et al. Contribution of redox-dependent activation of endothelial Nlrp3 inflammasomes to hyperglycemia-induced endothelial dysfunction. *J. Mol. Med.* **94**, 1335–1347 (2016).
18. Ma, C. et al. Neutrophil membrane-engineered Panax ginseng root-derived exosomes loaded MiRNA 182-5p targets NOX4/Drp-1/NLRP3 signal pathway to alleviate acute lung injury in sepsis: Experimental studies. *Int. J. Surg.* **110**, 72–86 (2024).
19. Lin, Y. K. et al. Salvianolic acid A from Danhong injection induces vasorelaxation by regulating L-type calcium channel in isolated mouse arteries. *J. Ethnopharmacol.* **296**, 115431 (2022).
20. Zuo, R. et al. Hepatic small extracellular vesicles promote microvascular endothelial hyperpermeability during NAFLD via novel-miRNA-7. *J. Nanobiotechnol.* **19**, 396 (2021).
21. Zhou, X. et al. Aspirin alleviates endothelial gap junction dysfunction through Inhibition of NLRP3 inflammasome activation in LPS-induced vascular injury. *Acta Pharm. Sin B.* **9**, 711–723 (2019).
22. Chen, C. A. et al. S-glutathionylation uncouples eNOS and regulates its cellular and vascular function. *Nature* **468**, 1115–1118 (2010).
23. Li, X. X. et al. Protective effects of acarbose against vascular endothelial dysfunction through inhibiting Nox4/NLRP3 inflammasome pathway in diabetic rats. *Free Radic Biol. Med.* **145**, 175–186 (2019).
24. Fang, J. et al. Hepatoma cell-secreted exosomal microRNA-103 increases vascular permeability and promotes metastasis by targeting junction proteins. *Hepatology* **68**, 1459–1475 (2018).
25. Huai, W. et al. Aryl hydrocarbon receptor negatively regulates NLRP3 inflammasome activity by inhibiting NLRP3 transcription. *Nat. Commun.* **5**, 4738 (2014).
26. Lee, Y. et al. Association of non-alcoholic steatohepatitis with subclinical myocardial dysfunction in non-cirrhotic patients. *J. Hepatol.* **68**, 764–772 (2018).
27. Cetindağlı, I. et al. Evaluation of endothelial dysfunction in patients with nonalcoholic fatty liver disease: Association of Selenoprotein P with carotid intima-media thickness and endothelium-dependent vasodilation. *Clin. Res. Hepatol. Gastroenterol.* **41**, 516–524 (2017).
28. Bai, B. et al. NLRP3 inflammasome in endothelial dysfunction. *Cell. Death Dis.* **11**, 776 (2020).
29. Zhang, Y., Chen, Y., Zhang, Y., Li, P. L. & Li, X. Contribution of cathepsin B-dependent Nlrp3 inflammasome activation to nicotine-induced endothelial barrier dysfunction. *Eur. J. Pharmacol.* **865**, 172795 (2019).
30. Gao, H. et al. MiR-690 treatment causes decreased fibrosis and steatosis and restores specific Kupffer cell functions in NASH. *Cell. Metab.* **34**, 978–990e4 (2022).
31. Hochreuter, M. Y., Dall, M., Treebak, J. T. & Barrès, R. MicroRNAs in non-alcoholic fatty liver disease: Progress and perspectives. *Mol. Metab.* **65**, 101581 (2022).
32. Liu, X. et al. Lipotoxic hepatocyte-derived Exosomal MicroRNA 192-5p activates macrophages through Rictor/Akt/Forkhead box transcription factor O1 signaling in nonalcoholic fatty liver disease. *Hepatology* **72** (2020).
33. Liu, X. et al. TMAO-activated hepatocyte-derived exosomes impair angiogenesis via repressing CXCR4. *Front. Cell. Dev. Biol.* **9**, 804049 (2022).
34. Hill, M. & Tran, N. MiRNA interplay: Mechanisms and consequences in cancer. *Dis. Model. Mech.* **14**, dmm047662 (2021).
35. Bock, K. W. Functions of Aryl hydrocarbon receptor (AHR) and CD38 in NAD metabolism and nonalcoholic steatohepatitis (NASH). *Biochem. Pharmacol.* **169**, 113620 (2019).

Acknowledgements

This work was funded by the following funds: the National Natural Science Foundation of China [82274130]; Chinese Medicine Guangdong Laboratory Science and Technology Development Project [HQL2024PZ006];

Key Research Platforms and Projects of Universities in Guangdong Province [2021ZDZX2041]; State Key Laboratory of Traditional Chinese Medicine Syndrome Graduate Program [SKLKY2024A0005]; Guangdong Province College Youth Innovative Talent Project [2024KQNCX068].

Author contributions

Qiuhe Chen: Methodology, Data analysis, Writing-original draft. Lifeng Ye: Investigation, Data collection; Liting Huang: Writing-review & editing; Hongjing You: Pearson's correlations analysis; Xiaoying Yu: Writing-review & editing; Ke Wang: Writing-review & editing; Shengtao Xiong: Writing-review & editing; Weiyan Liao: Writing-review & editing; Haiyan Li: Writing-review & editing; Xiao Wang: Project supervision; Chen Yang: Conceptualization, project administration & supervision.

Declarations

Competing interests

The authors declare no competing interests.

Additional information

Supplementary Information The online version contains supplementary material available at https://doi.org/10.1038/s41598-025-94917-y.

Correspondence and requests for materials should be addressed to Y.C.

Reprints and permissions information is available at www.nature.com/reprints.

Publisher's note Springer Nature remains neutral with regard to jurisdictional claims in published maps and institutional affiliations.